

LIQUEFACTION POTENTIAL EVALUATION IN TOBA CRATER INDONESIA

Karina Puspa Amalia¹, *Sito Ismanti², Ashar Saputra³

^{1,2,3} Department of Civil and Environmental Engineering, Faculty of Engineering, Universitas Gadjah Mada, Indonesia

*Corresponding Author, Received: 23 June 2023, Revised: 24 July 2023, Accepted: 4 Aug. 2023

ABSTRACT: Lake Toba Crater, specifically Samosir Island, Indonesia, is a caldera formed by the supervolcano eruption of Mount Toba. Furthermore, the region is susceptible to active earthquakes due to the presence of the Sumatran fault. Along the coastline, the soil is predominantly sandy, with a high groundwater level. These factors, namely earthquake and soil conditions, are reported to be the major triggering factors for a phenomenon known as liquefaction. According to the Indonesian Liquefaction Vulnerability Zone, Samosir Island is situated in a vulnerable area with medium potential. Therefore, this study aims to evaluate the liquefaction potential in Lake Toba Crater by taking a study case in the Culinary Building. Due to the SF site class of the study location, Site-Specific Response Analysis (SSRA) was required based on the Indonesian National Standard. A non-linear SSRA was used to determine the seismic wave propagation with DEEPSOIL v7. The analysis considered an earthquake exceedance probability of 2% in 50 years. The input parameters for the ground motion were obtained from the modification of 12 pairs of recorded data. The Peak Ground Acceleration value for each depth was generated from SSRA and used for liquefaction potential evaluation. This study used empirical methods, as well as two scenarios, namely maximum and frequent earthquakes with magnitudes of 6.4 M_w and 5.6 M_w , respectively. Based on the results, the area had liquefaction potential at 6-20 meters below the surface. The vulnerability level, as assessed using LPI value, was found to be very high, ranging from 25.71 to 56.51.

Keywords: Liquefaction, Liquefaction potential, Site response analysis, Peak ground acceleration, Lake Toba

1. INTRODUCTION

The eruption of Mount Toba in North Sumatra, Indonesia, approximately 74 thousand years ago, has led to the formation of a caldera, which consists of Samosir Island in its center. Moreover, the location of this region poses a relatively high seismic risk. This is primarily due to the presence of the Sumatran Fault, which crosses along the Sumatra island, as shown in Figure 1. It is recognized as a right-lateral strike-slip fault with a length of 1,900 km and 19 significant segments. It is also widely known for producing earthquakes with magnitudes greater than 7 M_w [1]. Several studies have reported that it is responsible for earthquakes and consists of several faults, including Toru and Renun, being the closest to the Toba region [2].

Based on the geotechnical investigation, the soil layer at Samosir Island consists of very loose to dense sand, with a depth of approximately 24 m . The area also experiences a high groundwater level (GWL) due to its location at the edge of Lake Toba.

Several studies have reported that earthquakes and soil conditions are triggering factors for the occurrence of liquefaction. Furthermore, the seismic and geological conditions at the study location showed that it was included in the

liquefaction-prone category. According to the Indonesian Liquefaction Vulnerability Zone, Samosir Island is situated within the vulnerable zone, with medium potential [3].

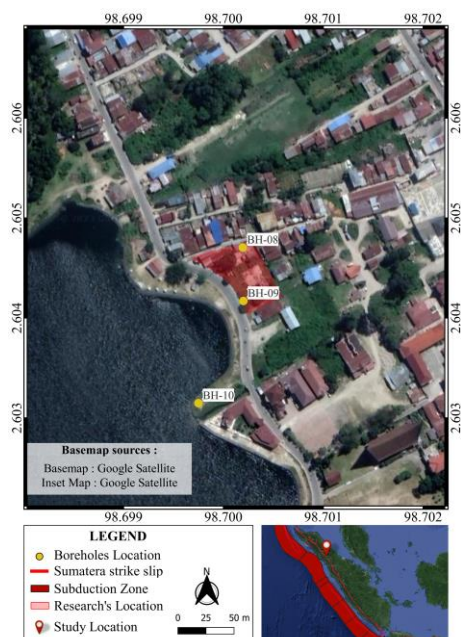


Fig.1 Study Location (taken from QGIS Software)

Liquefaction is a phenomenon that occurs when sandy, saturated soil experiences an increase in water pressure due to the application of an earthquake load. The excess pore water pressure causes a reduction or elimination of effective stress, leading to the softening or melting of the soil [4]. Several factors have been known to trigger liquefaction, including the intensity and duration of the earthquake, the type of soil, and the depth of groundwater level [5]. According to [6], soil conditions that are prone to liquefaction failure are included in the specific site class conditions Site Class-F category. Therefore, Site-Specific Response Analysis (SSRA) is often required to assess potential properly.

Several studies have been carried out on the evaluation of liquefaction potential in Indonesia. [7,8] conducted a potential analysis in Banda Aceh City and declared it as a region with high risk. In Palu City, Central Sulawesi, the western and southern parts were reported to have extremely high risk [9]. Furthermore, the Southern and Northern sides of Yogyakarta were found to have liquefaction [10,11]. Based on previous findings, there are no studies on the evaluation of liquefaction potential in Samosir Island, North Sumatra. Therefore, this study aims to evaluate the liquefaction potential in Samosir Island, as well as classify its level of vulnerability. SSRA was used to determine the PGA value, which was one of the important parameters during the assessment. Liquefaction potential investigation was performed using empirical methods by comparing the Cyclic Resistance Ratio (CRR) and Cyclic Stress Ratio (CSR) values at each depth. These values were then used to obtain the Safety Factor (SF) value, which was utilized in calculating the Liquefaction Potential Index (LPI).

2. RESEARCH SIGNIFICANCE

This study focused on analyzing the potential for liquefaction and its level of vulnerability using the PGA value obtained from SSRA results in the Crater of Lake Toba, Samosir Island. The results were expected to contribute to mitigating liquefaction disasters, as well as reducing risks to humans and damage to infrastructure. Evaluating the risk involved is the first step in determining the type of damage and the adequate preventive measures.

3. SITE ANALYSIS

3.1 Study Area

This study was carried out in Samosir Island, one of the five developments of the National Tourism Strategic Area, which was the

government's super-priority program in tourism development. This location was planned to be the center of a new tourist destination with a high spike of visitors, indicating that the risk of disaster was in line with the increase in activities. In addition, several buildings were built in the area to support the tourism function. This study focused on one of them, known as the Culinary Center Building. The N-SPT value obtained from soil investigations conducted in 2020 was used in this study. The distribution of borehole location is presented in Figure 1.

3.2 Geological Conditions

Samosir Island was originally a dome that collapsed due to the empty magma chamber after the eruption of Mount Toba. The collapse of the dome formed the Toba Caldera, which was later filled with the caldera wall avalanche, characterized by their steep and unstable nature. Moreover, fluvial sedimentation from the surrounding rivers contributed to the filling process. The base of the caldera was lifted to form Samosir Island due to the upward pressure of magma, which caused the top surface to dip slightly to the west (5-8°). Evidence of lake sediments in the form of thick diatoms could be observed on Samosir Island [12].

Samosir Island was dominated by the Samosir Formation (Qps), consisting of tuffaceous sandstones, siltstones, conglomerates, and diatomaceous. Meanwhile, alluvium sedimentary rocks (Qh) gravels, sands, muds, and conglomerates could be found along the coastline. The study location was situated on the edge of Samosir Island, which had quaternary young alluvium (Qh) deposits with sand dominance [13].

3.3 Geotechnical Conditions

Interpretation of the soil layers was carried out based on drill tests in cross-section, as shown in Figure 2. The study area was dominated by coarse to fine sand with loose to dense properties. At a certain depth, there were several inserts, such as on BH-08, which had a sandy silt layer at 20-22 m below the surface. Meanwhile, BH-10, located at the edge of the lake, had a layer of silt clay on the top. Based on the observation results, the study location was prone to liquefaction because it was dominated by sandy soils.

The average N-SPT value at the study site was 14, and values <20 indicated susceptibility to liquefaction with a high potential for structural damage [14]. Moreover, the groundwater level was less than 10 m, which was one of the significant factors contributing to the occurrence of liquefaction [15]. The grain size distribution plotted on the range curve for soils proposed by [16]

showed that the soil gradation at the study site was included in the category with liquefaction susceptibility, as shown in Figure 3.

Based on the conditions above, the soil profile was classified as SF site class. The SF site class consisted of soils that exhibited specific conditions associated with characteristics, such as susceptibility to failure or collapse due to earthquake loads, such as easy liquefaction. This category of soil often required SSRA [6].

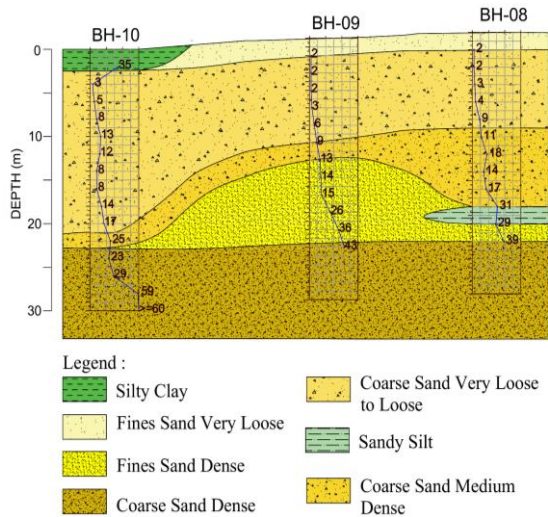


Fig.2 Soil layer interpretation

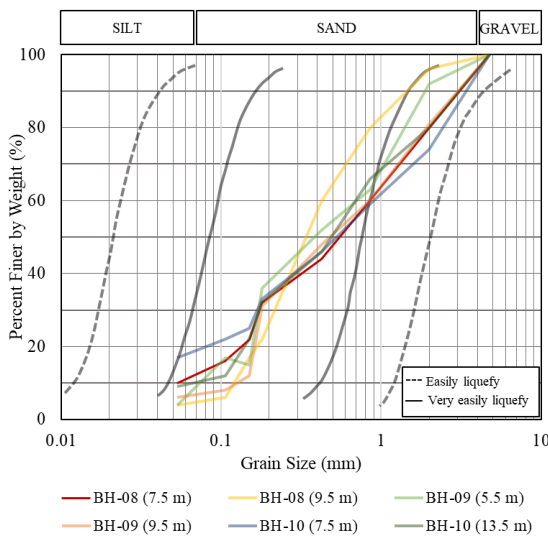


Fig.3 Grain size distribution in this study against grain size limit for liquefaction proposed by [16]

4. METHODOLOGY

4.1 Site-Specific Response Analysis (SSRA)

SSRA was used to determine the propagation of seismic waves from the bedrock to the surface, as well as the specific response conditions of the soil

in an area. It was also used to obtain the propagation of PGA values based on the soil layer characteristics. Furthermore, the PGA value obtained was used to evaluate liquefaction potential. It was also useful in the planning of earthquake-resistant buildings.

4.1.1 Modelling Approach

To observe the behavior of the soil against the earthquake loads, this study used the Non-Linear SSRA approach with time domain using DEEPSOIL v7 software to analyze one-dimensional (1-D) soil response. The DEEPSOIL v7 software was used to describe the GQ/H constitutive model, which was a hyperbolic model for calculating the soil backbone response describing the cyclic soil behavior [17]. The GQ/H method could explicitly describe the shear strength of the soil for each layer, which was unachievable with the previous MKZ method.

4.1.2 Input Motions

Due to the absence of ground motion records at the study location, a search was made from other locations in the PEER earthquake catalog with the same or close characteristics.

Ground motion selection and modification procedure must take into account the Earthquake Magnitude (M) and Source-to-site Distance (R) [18]. The determination of the M-R value at a certain location was carried out through PSHA analysis, namely disaggregation. In this study, the M-R values of the 4 earthquake source mechanisms, namely Megathrust, Benioff, shallow faults, and all sources, were obtained from [19] with a 2% exceedance probability in 50 years (2,475 years). The values were taken for peak acceleration vibration period, $S_a = 0.2 s$, and $S_a = 3.0 s$.

It was also important to consider the significant duration when collecting earthquake records that were relatively similar to one another [20]. This parameter referred to the length of a ground motion. Significant duration D595 was the interval over which a specified amount of energy dissipated within 5-95% of the total energy of an earthquake's ground acceleration. The D595 value was calculated using the equation proposed by [21].

Based on parameters obtained from [19], a total of 12 pairs of ground motions were selected for further amplitude scaling based on the spectral target from the Indonesian seismic code. A previous study revealed that a minimum of 11 pairs of earthquake time history must be utilized [20].

The target response spectrum for the MCER was obtained by multiplying the response spectrum design (Design-Based Earthquake-DBE) by a factor of 1.5 [6]. This study established the target response based on Probabilistic Seismic Hazard Analysis (PSHA). The response target of the MCER

spectrum for the study site is presented in Figure 4.

Amplitude scaling for the building was carried out in the fundamental period range of 0.2T1B-2T1A. In this study, the fundamental period value used was 0.1-1.46 s, and the results of the amplitude scaling showed a range of 0.5-4.4. Values less than 5 were recommended for the scaling process because the parameter did not represent the actual earthquake characteristics [22].

The synthetic ground motion result was used as the input motion in DEEPSOIL v7. The results of the selected ground motion recapitulation and the scaling factor are presented in Table 1. Meanwhile, spectral scaling results are shown in Figure 4.

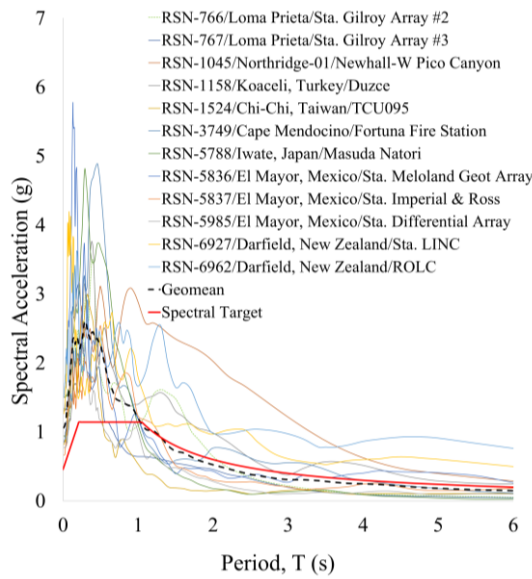


Fig.4 Scaled response spectrum

4.1.3 Soil Profile in Deep Soil

Site-specific soil profile based on geotechnical investigations is summarized in Table 2. To avoid

Table 1 Ground motion history

No	Code	Event	Station	Year	Mag	R	D595	Scaling Factor
1	RSN-766	Loma Prieta	Gilroy Array #2	1989	6.93	26.85	11.00	1.81
2	RSN-767	Loma Prieta	Gilroy Array #3	1989	6.93	31.40	11.40	1.48
3	RSN-1045	Northridge-01	Newhall - W Pico Canyon	1994	6.69	21.55	8.80	2.13
4	RSN-1158	Koaceli, Turkey	Duzce	1999	7.51	98.22	11.80	1.85
5	RSN-1524	Chi-Chi, Taiwan	TCU095	1999	7.62	95.70	13.30	1.30
6	RSN-3749	Cape Mendocino	Fortuna Fire Station	1992	7.01	30.04	15.00	2.14
7	RSN-5788	Iwate, Japan	Masuda Natori	2008	6.90	95.59	13.20	2.35
8	RSN-5836	El Mayor-Cucapah, Mexico	El Centro - Meloland Geot. Array	2010	7.20	55.28	24.70	2.05
9	RSN-5837	El Mayor-Cucapah, Mexico	El Centro - Imperial & Ross	2010	7.20	60.37	26.60	1.56
10	RSN-5985	El Mayor-Cucapah, Mexico	El Centro Differential Array	2010	7.20	60.65	13.80	1.40
11	RSN-6927	Darfield, New Zealand	LINC	2010	7.00	33.76	12.70	1.92
12	RSN-6962	Darfield, New Zealand	ROLC	2010	7.00	26.85	11.40	2.20

filtering out the dominant frequencies below 25-30 Hz in ground motion [23], the soil profile was discretized into certain density intervals. The shear wave velocity (V_s) was obtained from the correlation between vertical effective stress (σ'_{v0}) and N_{60} value with the equations proposed by [24], as shown below in Eq. 1 and Eq. 2.

for sand soil types

$$\ln(V_s) = 4.045 + 0.096 \ln(N_{60}) + 0.236 \ln(\sigma'_{v0}) \quad (1)$$

for silt soil types

$$\ln(V_s) = 3.783 + 0.178 \ln(N_{60}) + 0.164 \ln(\sigma'_{v0}) \quad (2)$$

The shear strength of each layer must be counted when using the GQ/H model to simulate soil behavior under large strains. The shear strength value was determined using the Mohr-Coulomb equation presented below in Eq. 3.

$$\tau = c_{vs} \sigma'_v \tan \phi \quad (3)$$

Where σ'_v is effective stress at the middle of the depth soil layer, ϕ is the friction angle, and c_{vs} is judgment-based shear strength. The c_{vs} value was calculated based on Eq. 4 using the input soil density (ρ) and shear wave velocity (V_s).

$$c_{vs} = \rho V_s^2 * 0.8 * 0.1\% \quad (4)$$

Apart from the parameters listed above, the reference soil dynamic curves proposed by [25] were also selected. This selection required a Plasticity Index (PI) and coefficient of earth pressure at rest (K_0). Furthermore, the K_0 value was obtained from Eq. 5 by inputting the value of the over-consolidation ratio (OCR) [26], which was 1.0 [25].

$$K_0 = [1 - \sin(\phi)] * OCR^{\sin(\phi)} \quad (5)$$

Table 2 Soil profile properties for BH-08

Layer	Depth (m)	Thickness (m)	N ₆₀	N ₁₍₆₀₎	σ _{vc} (kPa)	σ' _{vc} (kPa)	V _s (m/s)	ϕ	c _{vs}	τ	K ₀ (kPa)
1	0.5	0.5	2	3.32	6.68	6.68	95.54	27.14	9.94	13.36	0.54
2	1	0.5	2	3.32	13.35	13.35	112.52	27.14	13.79	20.63	0.54
3	2	1	2	3.32	26.70	26.70	132.52	27.14	19.12	32.81	0.54
4	3	1	2	3.32	40.05	40.05	145.83	27.14	23.16	43.69	0.54
5	4	1	2	2.91	53.40	53.40	156.07	26.70	26.53	53.38	0.55
6	4.8	0.8	2	2.54	64.08	64.08	162.93	26.25	28.91	60.52	0.56
7	5.6	0.8	2	2.54	74.76	68.69	165.63	26.25	29.88	63.76	0.56
8	6	0.4	3	3.48	80.15	71.06	173.59	27.32	33.14	69.85	0.54
9	7	1	4	4.53	93.77	77.14	181.94	28.36	36.76	78.39	0.53
10	8	1	4	4.34	107.38	83.22	185.22	28.17	38.10	82.67	0.53
11	9	1	9	9.26	121.65	90.06	203.99	31.94	48.44	104.59	0.47
12	10	1	9	8.90	135.92	96.91	207.54	31.71	50.14	110.01	0.47
13	11	1	11	10.47	150.45	104.06	215.17	32.70	54.89	121.69	0.46
14	12	1	11	10.11	164.99	111.21	218.57	32.48	56.64	127.42	0.46
15	13	1	18	16.11	180.44	119.44	233.04	35.75	68.47	154.45	0.42
16	14	1	18	15.59	195.89	127.67	236.74	35.50	70.65	161.70	0.42
17	15	1	14	11.65	210.82	135.29	234.27	33.40	66.84	156.02	0.45
18	16	1	14	11.31	225.75	142.90	237.32	33.20	68.59	162.09	0.45
19	17	1	17	13.48	241.07	150.98	244.94	34.41	74.99	178.40	0.43
20	18	1	17	13.11	256.40	159.05	247.97	34.21	76.86	184.99	0.44
21	19	1	31	24.44	273.56	169.28	266.59	39.40	99.51	238.56	0.37
22	20	1	31	23.80	290.72	179.51	270.31	39.15	102.30	248.42	0.37
23	21	1	29	21.53	307.62	189.43	272.01	38.21	102.01	251.13	0.38
24	22	1	29	21.01	324.52	199.35	275.31	37.99	104.50	260.18	0.38
25	23	1	39	28.85	342.74	210.81	287.01	41.08	122.41	306.18	0.34
26	24	1	39	28.19	360.95	222.27	290.62	40.84	125.50	317.60	0.35

4.2 Liquefaction Potential Analysis

4.2.1 Simplified Procedure

One of the methods used to evaluate liquefaction potential involved the use of InSite Test data, such as N-SPT data. This approach also required obtaining CSR value caused by an earthquake. A method that could be used to estimate CSR value based on maximum earthquake acceleration at the surface of the study location was proposed by [27], as presented in Eq. 6-9.

$$CSR_{M;\sigma'_{vc}} = 0.65 \frac{\alpha_{max}}{g} \frac{\sigma}{\sigma'} r_d \quad (6)$$

$$r_d = \exp[\alpha(z) + \beta(z)M] \quad (7)$$

$$\alpha(z) = -1.012 - 1.126 \sin\left(\frac{z}{11.73} + 5.133\right) \quad (8)$$

$$\beta(z) = 0.106 + 0.118 \sin\left(\frac{z}{11.28} + 5.142\right) \quad (9)$$

Where α_{max} is the maximum ground acceleration, g is the acceleration due to gravity, σ is the total soil stress, σ' is the effective soil stress, r_d is the stress reduction coefficient, z is the depth, and M is the moment magnitude.

Maximum ground acceleration value (α_{max}) was one of the important parameters in determining CSR value due to the earthquake that occurred. In

this study, ground acceleration values for each depth were obtained from SSRA.

CSR value was then compared with the soil resistance value (CRR) to determine liquefaction, which was calculated based on Eq. 10-11 [27].

$$CRR_{M;\sigma'_{vc}} = CRR_{M=7.5;\sigma'_{vc}=1} * MSF * K_{\sigma} \quad (10)$$

$$CRR_{M=7.5;\sigma'_{vc}=1} = \exp\left(\frac{(N_1)_{60cs}}{14.1} + \left(\frac{(N_1)_{60cs}}{126}\right)^2 - \left(\frac{(N_1)_{60cs}}{23.6}\right)^3 + \left(\frac{(N_1)_{60cs}}{25.4}\right)^4 - 2.8\right) \quad (11)$$

Where MSF is the magnitude scaling factor, K_{σ} is the correction factor of overburden, and $(N_1)_{60cs}$ is the correction factor of fines content.

Based on the results of the comparison of CSR and CRR values as shown in Eq. 12, SF was obtained, where < 1 indicated liquefaction potential.

$$SF = \frac{CRR_{M=7.5;\sigma'_{vc}=1}}{CSR} \quad (12)$$

4.2.2 Liquefaction Potential Index (LPI)

LPI could be used to estimate the level of liquefaction potential using several parameters, such as soil layer thickness, depth, and SF value of

the liquefied soil layer. LPI analysis was carried out to a depth of 20 m below the surface, and the calculation was performed using Eq. 13-17.

$$LPI = \int_0^{20} F * W(z) dz \quad (13)$$

$$F = 0 ; SF > 1.0 \quad (14)$$

$$F = 1 - SF ; SF < 1.0 \quad (15)$$

$$W(z) = 0 ; z > 20 m \quad (16)$$

$$W(z) = 10 - 0.5z ; z < 20 m \quad (17)$$

LPI value obtained was classified into several categories to determine the level of liquefaction potential, as shown in Table 3.

Table 3 Liquefaction potential classification [28]

LPI Value	Categories
0	Non-liquefied
0 < LPI ≤ 2	Low
2 < LPI ≤ 5	Moderate
5 < LPI ≤ 15	High
LPI > 15	Very High

4.2.3 Earthquake Magnitude

Determining the magnitude of an earthquake is crucial as it is one of the triggering factors for liquefaction phenomena. In this study, two scenarios were used during liquefaction analysis. The first involved the largest earthquake recorded within the vicinity of the study location, which occurred in 1987 with a magnitude of 6.4 Mw, according to the USGS record. Meanwhile, the second scenario focused on frequent earthquakes or those that occurred frequently with a magnitude of 5.6 Mw. These events occurred between 1914-2014, up to a total of 1,165 times [29].

5. RESULT AND DISCUSSION

5.1 Peak Ground Acceleration

SSRA results using DEEPSOIL v7 software were presented in the form of graphs of acceleration of earthquake vibrations for each soil profile. The results of SSRA in BH-08 and BH-09 are shown in Figure 5.

At BH-08, the acceleration of earthquake vibrations that occurred in the bedrock had magnified from 0.64 g to 0.66 g at the surface. Meanwhile, the PGA in BH-09 increased from 0.64 g to 0.65 g. Based on these findings, the amplification factor obtained from the bedrock to the soil surface in BH-08 and BH-09 was 1.022 and 1.004 respectively. The PGA propagation values

recorded in both sites were almost the same due to the uniform type of soil, namely sandy soil. The PGA was as an input parameter to determine CRR in analyzing liquefaction potential at each depth.

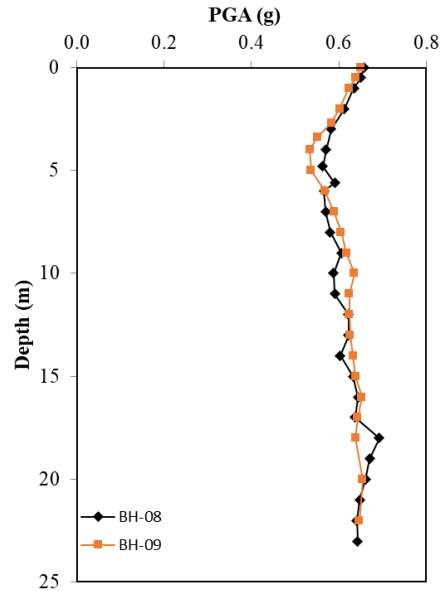


Fig.5 Average PGA of response profiles

5.2 Liquefaction Potential Evaluation

Liquefaction potential analysis in Lake Toba culinary center building was carried out on BH-08 and BH-09 based on the soil investigation performed in 2020. Based on that report, BH-08 and BH-09 predominantly contained sandy soil and GWL at a depth of -5.6 m and -2.7 m, respectively. GWL value used for the calculation of CSR.

BH-08 and BH-09 had a Fines Content (FC) value of < 15%. The top layer of soil in BH-08 was 0.6-7 m deep with an FC value of 9.83%. Meanwhile, the bottom layer had a depth of 8-24 m with an FC value of 3.81%. Compared to BH-08, BH-09 had an FC value of 4.42% and 5.98% at a depth of 0-8 m and 9-24 m, respectively. The low value was caused by the dominance of fine and coarse sand layers with loose to very loose densities. The sandy soil type at the study site was also due to its proximity to the edge of the lake with young alluvium deposits.

Based on two scenarios of an earthquake and PGA value for each depth from SSRA results, liquefaction potential analysis was carried out for BH-08 and BH-09. Analysis was calculated to a depth of 20 m based on the method proposed by [30]. The calculation results of liquefaction potential at BH-08 with an earthquake magnitude of 6.4 Mw are presented in Table 4.

Figure 6 shows the N-SPT and SF values for each depth in BH-08. Based on calculation under the moment magnitude scenario of 6.4 Mw, an SF

range of 0.25-0.71 was obtained at a depth of 6-20 m. This indicated that there was potential for liquefaction in this layer. Meanwhile, the liquefied layer was at the same depth for an earthquake scenario of 5.6 Mw, which was 6-20 m. The soil layer above the 5.6 m groundwater level did not experience any liquefaction potential, as the condition only occurred in saturated areas. Table 4 shows the calculation results of BH-08 under the 6.4 Mw scenario. It also elucidated the trend of increment in the PGA value, which caused an increase in CSR value as well as a decrease in SF.

The summary of SF values at BH-09 caused by moment magnitudes of 6.4 Mw and 5.6 Mw is presented in Figure 7. At a depth of 0 to 20 m, the ratio of CRR and CSR values was still below 1, with a range of 0.20-0.97. Therefore, there was liquefaction potential at this depth. Similar to BH-08, the results showed that the soil layer above GWL had no potential.

SF value obtained was used to calculate LPI using Eq. 13-17. LPI calculation on BH-08 and BH-09 was carried out up to a depth of 20 m. Based on the results, an earthquake of 5.6 Mw and 6.4 Mw caused a very high level of liquefaction potential in BH-08 with an LPI of 25.71 and 28.60, respectively. Meanwhile, values of 54.22 and 56.51

were obtained in BH-09. LPI on BH-09 was almost two times higher than that of BH-08 because the groundwater level was shallower, leading to the presence of more liquefied layers.

6. CONCLUSION

Soil layers under the culinary building in Toba Crater, Samosir Island was dominated by sandy soil types with a low groundwater level of 2.7 and 5.6 m below the surface, thereby causing liquefaction potential. Furthermore, liquefaction potential analysis was conducted at two boreholes (BH-08 and BH-09) in the culinary building using simplified procedures and the LPI method. Based on the scenario of maximum and frequent earthquakes of 6.4 and 5.6 Mw, along with PGA at each depth generated by SSRA, the study location had a very high level of vulnerability. Liquefaction potential was found at 2.7-20 m depth below the surface, with LPI ranging from 25.71 to 56.51.

Analysis results of liquefaction potential could be used as a reference in carrying out mitigation against this condition. However, further analysis was needed to determine the appropriate type of mitigation.

Table 4. Calculation of the liquefaction potential of BH-08 using 6.4 Mw earthquake scenario

Depth (m)	N-SPT	FC (%)	α	β	rd	PGA	CSR	(N ₁) _{60cs}	MSF	$K\sigma \leq 1.1$	CRR	SF	Exp
0.5	2	9.83	n.a	n.a	n.a	0.66	n.a	n.a	n.a	n.a	n.a	n.a	n.a
1	2	9.83	n.a	n.a	n.a	0.65	n.a	n.a	n.a	n.a	n.a	n.a	n.a
2	2	9.83	n.a	n.a	n.a	0.63	n.a	n.a	n.a	n.a	n.a	n.a	n.a
3	2	9.83	n.a	n.a	n.a	0.61	n.a	n.a	n.a	n.a	n.a	n.a	n.a
4	2	9.83	n.a	n.a	n.a	0.58	n.a	n.a	n.a	n.a	n.a	n.a	n.a
4.8	2	9.83	n.a	n.a	n.a	0.57	n.a	n.a	n.a	n.a	n.a	n.a	n.a
5.6	2	9.83	n.a	n.a	n.a	0.56	n.a	n.a	n.a	n.a	n.a	n.a	n.a
6	3	9.83	-0.34	0.04	0.91	0.59	0.36	4.53	1.05	1.02	0.08	0.25	L
7	4	9.83	-0.42	0.05	0.89	0.57	0.37	5.46	1.05	1.01	0.09	0.26	L
8	4	3.81	-0.50	0.06	0.87	0.57	0.39	4.21	1.05	1.01	0.08	0.22	L
9	9	3.81	-0.59	0.07	0.85	0.58	0.40	9.02	1.07	1.00	0.11	0.30	L
10	9	3.81	-0.68	0.08	0.82	0.61	0.43	8.68	1.07	1.00	0.11	0.27	L
11	11	3.81	-0.77	0.09	0.80	0.59	0.42	10.24	1.08	0.99	0.12	0.31	L
12	11	3.81	-0.87	0.10	0.78	0.59	0.42	9.89	1.08	0.99	0.12	0.30	L
13	18	3.81	-0.96	0.11	0.76	0.62	0.44	15.82	1.14	0.98	0.16	0.41	L
14	18	3.81	-1.06	0.12	0.74	0.62	0.44	15.32	1.14	0.97	0.16	0.40	L
15	14	3.81	-1.16	0.13	0.71	0.60	0.42	11.44	1.09	0.97	0.13	0.32	L
16	14	3.81	-1.25	0.14	0.69	0.63	0.43	11.12	1.09	0.96	0.13	0.31	L
17	17	3.81	-1.34	0.15	0.67	0.64	0.43	13.27	1.11	0.95	0.14	0.35	L
18	17	3.81	-1.43	0.16	0.65	0.64	0.42	12.91	1.11	0.95	0.14	0.35	L
19	31	3.81	-1.52	0.17	0.64	0.69	0.45	24.15	1.28	0.91	0.27	0.71	L
20	31	3.81	-1.61	0.18	0.62	0.67	0.42	23.53	1.27	0.91	0.26	0.71	L
21	29	3.81	n.a	n.a	n.a	0.66	n.a	n.a	n.a	n.a	n.a	n.a	n.a
22	29	3.81	n.a	n.a	n.a	0.65	n.a	n.a	n.a	n.a	n.a	n.a	n.a
23	39	3.81	n.a	n.a	n.a	0.64	n.a	n.a	n.a	n.a	n.a	n.a	n.a
24	39	3.81	n.a	n.a	n.a	0.64	n.a	n.a	n.a	n.a	n.a	n.a	n.a

Note: L is Liquefied, n.a. is Not Available

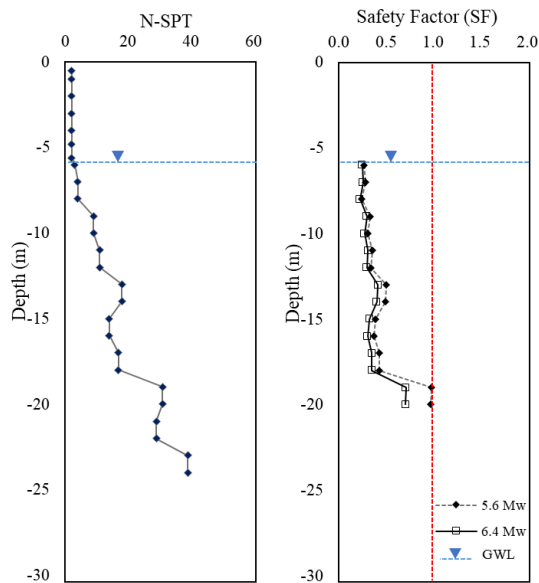


Fig.6 Results of liquefaction SF BH-08

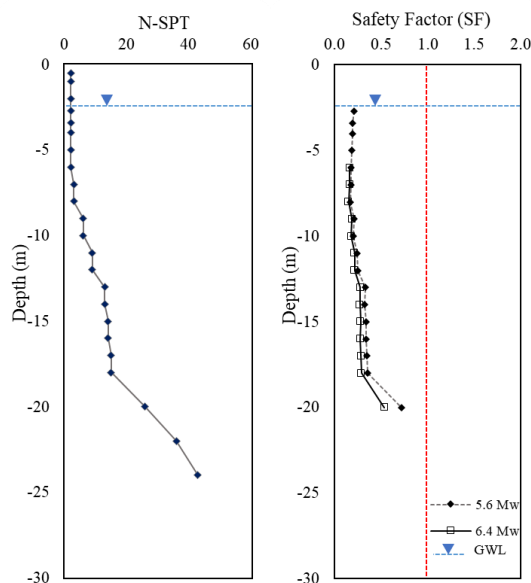


Fig.7 Results of liquefaction SF BH-09

7. ACKNOWLEDGMENTS

The authors are grateful to the Ministry of Public Works and Housing, the Directorate of Settlement Area Development, and the Settlement Infrastructure Agency for Sumatera Region for their assistance with the data and all aspects of this study.

8. REFERENCES

[1] Sieh, Kerry, and Danny Natawidjaja, Neotectonics of the Sumatran Fault, Indonesia, *Journal of Geophysical Research: Solid Earth* Vol. 105 No B12, 2000, pp. 28295-28326.

[2] National Center for Earthquake Studies: Indonesian Seismic Sources and Seismic Hazard Maps, Center for research and development of housing and resettlement. Ministry of Public Works and Human Settlements, 2017.

[3] Ministry of Energy and Mineral Resources, Map of Indonesia's Liquefaction Vulnerability Zone, 2019.

[4] Srbulov, Milutin, *Geotechnical Earthquake Engineering: Simplified Analyses with Case Studies and Examples*, Geotechnical, Geological, and Earthquake Engineering 9. Dordrecht: Springer, 2008.

[5] Day, R. W., *Geotechnical Earthquake Engineering Handbook*, United States, 2012, pp. 1-500.

[6] Indonesian Standard Code, *Earthquake Resistance Design for Buildings (SNI 03-1726-2019)*, National Standardization Agency, 2019.

[7] Jalil, A., Fathani, T. F., Satyarno, I., and Wilopo, W., A Study on the Liquefaction Potential in Banda Aceh City after the 2004 Sumatera Earthquake, *International Journal of GEOMATE*, Vol. 18, Issue 65, 2020, pp. 147-155.

[8] Syukri, M., Anda, S. T., Safitri, R., Fadhli, Z., and Saad, R., Prediction of Soil Liquefaction Phenomenon in Banda Aceh and Aceh Besar, Indonesia Using Electrical Resistivity Tomography (ERT). *International Journal of GEOMATE*, Vol. 18, Issue 70, 2020, pp. 123-129.

[9] Patriaman, F., Fathani, T. F., Wilopo, and W., Liquefaction Potential Analysis in Palu Bay Area, in *Proc. 4th International Conference of Water Resources Development and Environmental Protection (ICWRDEP 2021)*, Vol. 930, 2021.

[10] Hartono, N., and Fathani, T.F., The Using of GIS to Delineate the Liquefaction Susceptibility Zones at Yogyakarta International Airport, *Civil Engineering Dimension*, Vol. 24, No. 1, 2022, pp. 62-70.

[11] Kevin, P., Muhrozi, The Preliminary Study of Liquefaction Susceptibility Map in the Yogyakarta-Bawen Toll Road Sections I and II, Indonesia, *Civil Engineering Dimension*, Vol. 25, No. 1, 2023, pp. 29-36.

[12] Chesner, Craig A., *The Toba Caldera Complex*, Quaternary International, Vol. 258, 2012, pp. 5-18.

[13] Aldiss, D. T., Whandoyo, R., Ghazali, S. A., and Kusyono. *Geologic Map of the Sidikalang and (part of) Sinabang Quadrangles, Sumatra*. scale 1:250.000, Geol. Surv. of Indonesia, Ministry of Mines, Jakarta, 2011.

[14] Seed, H. B., Tokimatsu, K., and Chung, R. M.,

- Influence of SPT Procedures in Soil Liquefaction Resistance Evaluations. *Journal of Geotechnical Engineering*, Vol. 111, No. 12, 1985, pp. 1425-1445.
- [15] Youd, T. L., Tinsley, J. C., Perkins, D. M., King, E. J., and Preston, R. F., Liquefaction Potential Map of San Fernando Valley, California, in *Proc. The Second International Conference on Microzonation for Safer Construction-Research and Application*, Vol. I, 1979, pp. 37-48.
- [16] Tsuchida, H., Estimation of Liquefaction Potential of Sandy Soils and Countermeasures Against Liquefaction, in *Proc. Annual Meeting of the Port and Harbour Research Institute*, 1970. pp. (3-1)-(3-33).
- [17] Groholski, D. R., Hashash, Y. M. A., Kim, B., Musgrove, M., Harmon, J., and Stewart, J. P., Simplified Model for Small-Strain Nonlinearity and Strength in 1D Seismic Site Response Analysis, *Journal of Geotechnical and Geoenvironmental Engineering*, Vol. 142, Issue 9, 2016, pp. 04016042
- [18] Bommer, J. J., and Acevedo, A. B., The Use of Real Earthquake Accelerograms as Input to Dynamic Analysis, *Journal of Earthquake Engineering*, Vol. 8, Issue sup001, 2004, pp. 43-91.
- [19] Ministry of Public Works and Housing, *Earthquake Disaggregation Book 2022 For Planning and Evaluation of Earthquake Resistant Infrastructure*, 2022.
- [20] Indonesian Standard Code, *Procedure for Ground Motion Selection and Modification for Earthquake Resistance Design for Buildings (SNI 8899-2020)*, National Standardization Agency of Indonesia, 2020.
- [21] Kempton, J. J., and Stewart, J. P., Prediction Equations for Significant Duration of Earthquake Ground Motions Considering Site and Near-Source Effects, *Earthquake Spectra*, Vol. 22 (4), 2006, pp. 985-1013.
- [22] Zareian, F. and Zhong, P., *Ground Motion Selection and Scaling for the Analysis of the Tall Building Case Studies*. PEER., 2010.
- [23] Hashash, Y. M. A., Groholski, D. R., and Phillips, C., Recent Advances in Non-Linear Site Response Analysis, in *Proc. 5th International Conference on Recent Advance in Geotechnical Earthquake Engineering and Soil Dynamics and Symposium in Honor of Professor I. M. Idriss*, 2010.
- [24] Brandenburg, Scott J., Naresh Bellana, and Thomas Shantz., Shear Wave Velocity as Function of Standard Penetration Test Resistance and Vertical Effective Stress at California Bridge Sites, *Soil Dynamics and Earthquake Engineering*, Vol. 30, Issue 10, 2010, pp. 1026-1035.
- [25] Darendeli, M. B., Development of a new Family of Normalized Modulus Reduction and Material Damping Curves, *Civil Engineering*. Austin: University of Texas at Austin ProQuest Dissertations Publishing, 2001, pp 395.
- [26] Jaky J., Pressure in Silos, in *Proc. 2nd International Conference on Soil Mechanics and Foundation Engineering*, Rotterdam, Nederland, Vol. 1, 1948. pp. 103-107.
- [27] Boulanger, R. W., and Idriss, I. M., CPT and SPT Based Liquefaction Triggering Procedures, Rep. No. UCD/CGM-14/01, Univ. of California, Davis, CA, 2014.
- [28] Sonmez, H., Modification of the Liquefaction Potential Index and Liquefaction Susceptibility Mapping for a Liquefaction-Prone Area (Inegol, Turkey), *International Journal of Geosciences : Environmental Geology*, Vol. 44, Issue 7, 2003, pp. 862-871.
- [29] Asnita, Q., Sugiyanto, D., and Rusydy, I., Study of Statistical Seismicity on Sumatera Region, in *Proc. Indonesian Students Conference on Science and Mathematics (ISCSM)*, Vol. 16, No. 2, 2016.
- [30] Iwasaki, T., Arakawa, T., and Tokido, K.I., Simplified Procedures for Assessing Soil Liquefaction during Earthquakes, *International Journal of Soil Dynamics and Earthquake Engineering*, Vol. 3, Issue 1, 1984, pp. 49-58.